HHS Public Access

Author manuscript

J Immunol. Author manuscript; available in PMC 2021 July 30.

Published in final edited form as:

J Immunol. 2019 June 01; 202(11): 3187–3197. doi:10.4049/jimmunol.1900089.

Dlg1 Maintains Dendritic Cell Function by Securing Voltage-Gated K+ Channel Integrity

Xuejiao Dong[#*], **Lisi Wei**[#†], **Xueheng Guo**[#‡,§], **Zhiyong Yang**[¶], **Chuan Wu**[‖], **Peiyu Li**[#,**], **Lu Lu**[#], **Hai Qi**[‡], **Yan Shi**[‡], **Xiaoyu Hu**[‡], **Li Wu**[‡], **Liangyi Chen**[†], **Wanli Liu**[*]

[*]Ministry of Education Key Laboratory of Protein Sciences, Center for Life Sciences, Collaborative Innovation Center for Diagnosis and Treatment of Infectious Diseases, School of Life Sciences, Beijing Key Laboratory for Immunological Research on Chronic Diseases, Institute for Immunology, Tsinghua University, Beijing 100084, China;

[†]State Key Laboratory of Membrane Biology, Beijing Key Laboratory of Cardiometabolic Molecular Medicine, Institute of Molecular Medicine, Peking University, Beijing 100871, China;

[‡]Institute for Immunology, School of Medicine, Tsinghua University, Beijing 100084, China;

[§]National Education Examinations Authority, Beijing 100084, China;

[¶]Cardiovascular Research Institute, University of California, San Francisco, San Francisco, CA 94143;

[‖]Experimental Immunology Branch, National Cancer Institute, National Institutes of Health, Bethesda, MD 20851;

[#]Key Laboratory of Medical Molecular Virology of the Ministry of Education/Ministry of Health, School of Basic Medical Sciences and Shanghai Public Health Clinical Center, Fudan University, Shanghai 200032, China;

[**]Department of Infectious Diseases and Shenzhen Key Laboratory for Endogenous Infections, Shenzhen Nanshan People's Hospital, Guangdong Medical University, Shenzhen 518052, China

[#] These authors contributed equally to this work.

Abstract

Dendritic cells (DCs) play key roles in Ab responses by presenting Ags to lymphocytes and by producing proinflammatory cytokines. In this study, we reported that DC-specific knockout of discs large homologue 1 (Dlg1) resulted in a significantly reduced capacity to mediate Ab responses to both thymus-independent and thymus-dependent Ags in *Dlg1*$^{fl/fl}$Cd11c-Cre-GFP mice. Mechanistically, Dlg1-deficient DCs showed severely impaired endocytosis and

Address correspondence and reprint requests to Dr. Wanli Liu and Prof. Li Wu or Dr. Liangyi Chen, School of Life Sciences, Tsinghua University, Beijing 100084, China (W.L.) and School of Medicine, Tsinghua University, Beijing 100084, China (L. Wu) or State Key Laboratory of Membrane Biology, Beijing Key Laboratory of Cardiometabolic Molecular Medicine, Institute of Molecular Medicine, Peking University, Beijing 100871, China (L.C.). liulab@tsinghua.edu.cn (W.L.) and wuli@tsinghua.edu.cn (L. Wu) or lychen@pku.edu.cn (L.C.).

Disclosures

The authors have no financial conflicts of interest.

The online version of this article contains supplemental material.

phagocytosis capacities upon Ag exposure. In parallel, loss of Dlg1 significantly jeopardized the proinflammatory cytokine production by DCs upon TLR stimulation. Thus, Dlg1-deficient DCs lost their functions to support innate and adaptive immunities. At a cellular level, Dlg1 exhibited an indispensable function to maintain membrane potential changes by securing potassium ion (K^+) efflux and subsequent calcium ion (Ca^{2+}) influx events in DCs upon stimulation, both of which are known to be required for proper function of DCs. At a molecular level, Dlg1 did so by retaining the integrity of voltage-gated K^+ channels (including Kv1.3) in DCs. The loss of Dlg1 led to a decreased expression of K^+ channels, resulting in impaired membrane potential changes and, as a consequence, reduced proinflammatory cytokine production, compromised Ag endocytosis, and phagocytosis. In conclusion, this study provided, to our knowledge, a novel insight into Dlg1 and the voltage-gated K^+ channels axis in DC functions.

The production of Abs is an important function of human adaptive immunity. Dendritic cells (DCs), a link between innate and adaptive immunities, play key roles in Ab responses by capturing and presenting Ags to lymphocytes and by producing proinflammatory cytokines upon Ag stimulation (1). DCs can be classified into several distinct subsets, consisting of $CD8\alpha^+$ conventional DCs (cDCs), $CD11b^+$ cDCs, and plasmacytoid DCs (pDCs), according to their cell surface markers, anatomic locations, or immunological functions (2). Under physiological conditions, DCs usually form dynamic cell–cell contacts when performing their functions (3–5), which have been described as a specialized membrane structure named immunological synapse. In DC–T cell contacts, DCs present Ags to T cells and fine-tune T cell activation via surface receptors, costimulatory molecules, and secreted cytokines (3, 4). Ag-bearing DCs can also activate B cells by cell–cell contacts (5). DC immunological synapse is a typical highly polarized membrane structure, the formation of which involves the occurrence of molecular events to remodel the cytoskeleton and recruit a series of serine-threonine kinases, lipid kinases, and adaptor proteins, suggesting the highly dynamic nature of DC immunological synapse (4).

The Scribble complex, which is composed of Scribble, discs large (Dlg), and lethal giant larvae, is known to play key roles in highly polarized membrane structures, including epithelial cell junctions, neuronal synapses, B cell synapses, and T cell synapses (6–9). There are four members in the Dlg family, which are discs large homologue 1 (Dlg1) (SAP-97), Dlg2 (PSD-93), Dlg3 (SAP-102, NE-Dlg), and Dlg4 (PSD-95) (10). The Dlg family belongs to the membrane-associated guanylate kinase (MAGUK) superfamily, consisting of three PDZ domains, a single L27 domain, a single SH3 domain, and a guanylate kinase domain (11). In neurons, Dlg1 has been shown to play important roles in controlling signal strength and neuron receptor density through its interaction with cytoplasmic tails of neuronal α-amino-3-hydroxy-5-methyl-4-isoxazolepropionic acid receptor (AMPA) or *N*-methyl-D-aspartic acid receptor (NMDA) at neuronal synapses (11). In immunological studies, Dlg1 has been implicated in the functions of B cells and T cells, such as stabilizing the phosphatase and tensin homolog (PTEN) to suppress AKT activation (12) and recruiting p38 for NFAT activation (13). However, there is a lack of comprehensive studies to investigate the role of Dlg1 in the activation and functions of DCs, despite its sole high expression level among all four Dlg family members in DCs (14).

In this study, we investigated Dlg1 functions in DCs by deleting the *dlg1* gene from murine DCs. We found that Dlg1-deficient DCs exhibited a significantly reduced capacity to mediate Ab responses in scenarios of both thymus-independent (TI) and thymus-dependent (TD) Ag immunization. Mechanistically, we showed that this compromised function of DCs to support Ab responses is due to the severely impaired endocytosis and phagocytosis capacity of DCs upon Ag encounters and a significantly decreased ability to secret proinflammatory cytokines upon TLR stimulation. Thus, it was an intriguing finding that Dlg1 functions as a crucial gatekeeper to secure sufficient DC responses in both innate and adaptive immunities. Moreover, we provided molecular level evidence to show that the loss of Dlg1, consequently, led to a decreased cellular amount of voltage-gated K^+ channel subunits, which in turn jeopardized K^+ efflux, Ca^{2+} influx, and membrane potential dynamics in DCs upon stimulation, resulting in functional loss of DCs. Thus, all these results provided, to our knowledge, a novel insight into Dlg1 and the voltage-gated K^+ channel axis in ensuring DC functions in both innate and adaptive immunities.

Materials and Methods

Mice

Cd11c-Cre-GFP mice were acquired from The Jackson Laboratory (stock no. 007567, Cd11c-Cre-GFP line 4097). *Dlg1*$^{fl/fl}$ mice were a gift from Dr. S.K. Pierce (National Institutes of Health). All mice were maintained on C57BL/6 background and housed in a specific pathogen-free environment in the Animal Facility of Tsinghua University. Experiments were approved by the Animal Ethics Committee of Tsinghua University (approval no. 15-LWL2).

Isolation of splenic DCs and generation of bone marrow–derived DCs

Splenic DCs were purified as previously described (15). Briefly, splenic DCs were enriched by digesting tissue fragments with DNase I (Roche) and collagenase III (Worthington), followed by Ficoll–Paque (density 1.077 g/ml; GE Healthcare) separation and immunomagnetic bead depletion.

Bone marrow–derived DCs (BMDCs) were generated by culturing bone marrow cells (BMC; 2×10^5 cells/ml) in RPMI 1640 culture media supplemented with 10% FBS, penicillin, streptomycin, IL-4 (10 ng/ml, 51084-MNAE; Sino Biological), and GM-CSF (20 ng/ml, 315–03; PeproTech) for 7 d. $CD11c^+$ BMDCs were purified through incubation with CD11c–biotin (N418; Miltenyi Biotec) Abs, followed by positive selection via Streptavidin MicroBeads (Miltenyi Biotec).

Western blot

Whole cells were lysed by cell lysis buffer (Cell Signaling Technology no. 9803, 1 mM protease inhibitor mixture, and 1 mM PMSF) and then mixed with 4× loading buffer. Samples were then boiled for 10 min in water and separated by SDS-PAGE. Abs against IRF3, MyD88, p-Jnk, Jnk, IκBα, AKT, p-AKT (S473), and p-AKT (T308) were purchased from Cell Signaling Technology. Abs against Dlg1 (K64/15), pan-Kvβ potassium channel subunit (K40/17), Kv1.3 (L23/27), and Kv1.5 (K7/45) were purchased from Neuromab, and

anti–β-actin Abs were purchased from Bioeasy. Digital images were captured using the Amersham Image 600 system (GE Healthcare).

Flow cytometry

Single-cell suspensions were prepared. Cells were first blocked by using CD16/32 Ab (clone 2.4G2) and then were stained with a combination of the following Abs purchased from eBioscience and BioLegend: anti-CD11c (N418), anti-CD95 (15A7), anti–Siglec H (eBio440c), anti-CD8α (53−6.7), anti-F4/80 (T45-2342), anti-CD11b (M1/70), anti-CD103 (2E7), anti-MHC class II (MHC-II; M5/114.15.2), anti-CD24 (M1/69), anti-CD80 (16-10A1), anti-CD86 (GL1), anti-B220 (RA3-6B2), anti-GL7 (GL-7), and anti-TLR4 (SA15-21). An LSRFortessa (BD Biosciences) was used to acquire data. The data were analyzed and displayed by FlowJo software (Tree Star).

Ab titer analysis and cytokine detection

TD and TI Ag immunization and Ab titer analysis were performed as previously described (16). Briefly, for TD Ab response, mice were immunized by peritoneal injection of TD Ag 4-hydroxy-3-nitrophenylacetyl 33–keyhole limpet hemocyanin (NP_{33}-KLH; N-5060, 25 μg/mouse; Biosearch Technologies) mixed with CFA. Serum was collected every 2 wk, and 4-hydroxy-3-nitrophenylacetic (NP)–specific IgM and IgG were determined by ELISA. For TI Ab response, mice were immunized by peritoneal injection of 50 μg of NP–AminoEthylCarboxyMethyl–Ficoll (F-1420−10; Biosearch Technologies) per mouse. Serum was collected at the indicated time points, and NP-specific IgM was detected by ELISA. NP-BSA (ratio <20, N-5050H-10; Biosearch Technologies) or NP-BSA (ratio 5–9, N-5050L-10; Biosearch Technologies) were used for coating plate. For cytokine production assay, BMDCs (1×10^6) were plated in a six-well plate and then stimulated with the indicated stimulus for 6 h. ELISA kits were used to detect cytokines in collected supernatant. For in vivo administration, 1 μg of LPS (Sigma)/mouse was i.v. injected via tail veins. Serum was collected through tail vein bleeding 2 h later, centrifuged after coagulation, and stored at −20°C. ELISA kits were used to detect cytokines (88–7064, IL-6 [eBioscience]; 88–7324, TNF-α [eBioscience]; and 431604, IL-12p40 [BioLegend]), according to the manufacturers' instructions.

Ag uptake

The endocytosis experiment was performed as described in a previous protocol (16). Briefly, splenic cDCs were resuspended in prewarmed RPMI 1640 complete medium and incubated with Alexa Fluor 647 (AF647)–conjugated OVA (Molecular Probes O-34784) at a final concentration of 5 μg/ml for 30 min. Uptake of AF647-OVA was terminated by adding ice-cold PBS. The cells were washed three times by cold PBS before flow cytometry analysis.

Latex beads, carboxylate-modified polystyrene, and fluorescent red (L3030, diameter 2 μm; Sigma) were coated for 1 h at 37°C with mouse IgG (Jackson ImmunoResearch). After rinsing and reconstituting in RPMI 1640 complete medium, beads were added to BMDCs at a ratio of 10:1 (beads:BMDCs) and incubated with BMDCs for indicated time periods at 37°C. BMDCs were collected, washed in cold PBS to remove nonadherent beads, and fixed in 4% (w/v) polyoxymethylene. Cells were subjected to flow cytometry analysis.

Tumor model

Mice were s.c. injected with B16-F10 melanoma cells (5×10^5 cells per mouse). After 10 d, the volumes of tumors under skin were quantified with the following parameters (volume = width [millimeters] × width (millimeters) × length (millimeters)/2).

Reverse transcription and real-time PCR

Total RNA was isolated from 2×10^6 $CD11c^+$ BMDCs with indicated stimulation by TRIzol Reagent (Invitrogen). Reverse transcription was performed with the Revert Aid First Strand cDNA Synthesis Kit (Thermo Fisher Scientific). cDNA was analyzed by CFX96 real-time PCR system (BioRad) with reagents of SYBR Premix Ex Taq II (TaKaRa). The expression levels of target genes were determined by reference gene *Gapdh*. Statistical analysis was performed with $2^{-\Delta\Delta Ct}$ value. Primer sequences were as follows: *Gapdh* forward: 5′-TGTTCCTACCCCCAATGTGTC-3′; *Gapdh* reverse: 5′-TAGCCCAAGATGCCCTTCAGT-3′; *Il6* forward: GAGGA5′-TACCACTCCCAACAGACC-3′; *Il6* reverse: 5′-AAGTGCATCATCGTTGTTCATACA-3′; *Tnfa* forward: 5′-ATGGCCTCCCTCTCATCAGT-3′; *Tnfa* reverse: 5′-GCTCCTCCACTTGGTGGTTT-3′, *Il12b* forward; 5′-TGGTTTGCCATCGTTTTGCTG-3′; *Il12b* reverse: 5′-ACAGGTGAGGTTCACTGTTTCT-3′; *Kcna3* forward: 5′-GCAGTAGTAACCATGACAACT-3′; and *Kcna3* reverse: 5′-GCCCACAATCTTGCCTCCTA-3′.

Mass spectrometry sample preparation

$CD11b^+$ cDCs were isolated from murine spleens by MACS sorting as described previously (15). Each group of wild-type (WT) and knockout (KO) $CD11b^+$ cDCs were individually homogenized in 150 μl of urea lysis buffer (8 M urea in PBS, 1 mM protease inhibitor mixture, and 1 mM PMSF, pH 8). All sample homogenizations were performed by sonication. Briefly, each cell protein supernatant was added to urea lysis buffer in 1.5-ml tubes (MCT-150-C-S; Axygen) and sonicated (Diagenode) 12 times for 30 s with 30-s rest intervals. Subsequently, protein samples were centrifuged at 12,000 × *g* for 10 min, and sediment was discarded. All above procedures were done at 4°C or on ice. Protein concentration was determined by Bicinchonicnic Acid Kit (Tiangen) according to the manufacturer's protocol. Eighty micrograms of protein and 5 mM dithiotheitol were incubated at room temperature for 1 h, followed by trypsin digestion for 16 h at 37°C. Peptide purifying and labeling were done by Sep-Pak-C18 cartridges and tandem mass tag reagents (Thermo, Pierce Biotechnology). The labeled peptides were desalted by Sep-Pak C18 cartridges and then separated by reversed-phase chromatography. The peptides were separated into 12 fractions with high-pH reversed-phase liquid chromatography (XBridge BEH300 C18 5 μm [Waters], mobile phase A, 2% acetonitrile, pH 10; and mobile phase B, 98% acetonitrile, pH 10). The fractions were dried and redissolved in 20 μl of 0.1% formic acid (v/v) in water for second-dimension liquid chromatography–tandem mass spectrometry (MS) analysis.

Proteomic and gene ontology pathway analyses

Proteomic analyses were performed as a previous protocol described (17). The raw data generated by MS spectra were searched against the UniProt Mouse database (April 22, 2017; 59,594 sequences) using the SEQUEST search engine by Proteome Discoverer 2.2 software. Sum PEP Score (>3) was used as the first screening tool for the quality of data. Then, a ratio was calculated comparing KO and WT (KO/WT) groups, and at least a 1.3-fold or 0.7-fold change in both groups was identified. Gene ontology (GO) and Kyoto Encyclopedia of Genes and Genomes pathway database analyses were analyzed by DAVID (https://david.ncifcrf.gov/tools.jsp) with identified proteins from MS data. GOTERM_BP_DIRECT was exported for further analysis. Bubble plots were plotted with the bubble package in R software.

Electrophysiological experiments

Whole-cell patch clamp recordings were carried out using an EPC-10 amplifier (HEKA) at room temperature. Electrodes were pulled from borosilicate glass (outer diameter of 1.5 mm and inner diameter of 0.84 mm; Vital Sense Scientific Instruments) on a PP-830 puller (Narishige) with pipette resistance around 5–7 MΩ. The bath solution contained 150 mM NaCl, 5 mM KCl, 1 mM $MgCl_2$, 2.5 mM $CaCl_2$, 10 mM glucose, and 10 mM HEPES (pH 7.4, adjusted with NaOH). The pipette solution contained 134 mM KCl, 1 mM $CaCl_2$, 5 mM Na_2-ATP, 2 mM $MgCl_2$, 10 mM EGTA, and 10 mM HEPES (pH 7.2, adjusted with KOH). The whole currents were low-pass filtered at 2 kHz and sampled at 5 kHz before digitization. All recordings were routinely subtracted for leak currents at −70 mV online. Only cells with a series resistance compensation of 80–90% were selected for analysis. We used Igor Pro software (WaveMetrics) to analyze data and prepare final images.

Calcium influx

For detection of intracellular Ca^{2+} flux, BMDCs were preloaded with Indo-1 AM and probenecid (Molecular Probes; Invitrogen) in HBSS (Life Technologies) with 2% FBS at 30°C for 30 min. After collecting a baseline reading for 30 s, the indicated concentration of LPS was added to cells. The ratio of fluorescence (405/525 nm, violet/blue) was determined for 300 s on an LSR II (BD Biosciences).

Statistical analysis

Significant differences were analyzed by GraphPad Prism 7 following two-tailed (except where noted) Student *t* tests. Bars indicate mean 6 SEM. The *p* values $*p < 0.05$, $**p < 0.01$, $***p < 0.001$, and $****p < 0.0001$ indicate significant differences.

Results

Dlg1 is not essential for DC development and maturation

To investigate roles of Dlg1 in DCs, we depleted Dlg1 in cDCs by cross-breeding Cd11c-Cre-GFP mice with $Dlg1^{fl/fl}$ mice to generate $Dlg1^{fl/fl}$Cd11c-Cre-GFP mice. To confirm Dlg1 deficiency, subsets of splenic cDCs were isolated and subjected to Western blot analysis for Dlg1 expression. Compared to WT controls, Dlg1 in both $CD8\alpha^+$ and $CD11b^+$

cDCs from *Dlg1*$^{fl/fl}$Cd11c-Cre-GFP mice were considerably diminished (Fig. 1A). BMDCs originating from WT control mice showed high levels of Dlg1 expression, whereas Dlg1 was undetectable in Dlg1-KO BMDCs (Fig. 1A). Collectively, these results indicated successful KO of Dlg1 in cDCs.

We then sought to address the impact of Dlg1 deficiency on cDC development and maturation. The number of splenic CD8α$^+$ cDCs and CD11b$^+$ cDCs in spleens and in inguinal lymph nodes was unaffected (Fig. 1B, 1C). We next studied whether Dlg1-associated signals were required to promote the development of cDCs or precursor turnover. Culturing *Dlg1*$^{fl/fl}$Cd11c-Cre-GFP BMC with GM-CSF (Supplemental Fig. 1A) or Flt3 ligand (Supplemental Fig. 1B, 1C) generated DC populations with a phenotype indistinguishable from that of Cd11c-Cre-GFP DCs. These results showed that Dlg1 was not required for BMDC generation.

To investigate whether Dlg1 affected DC maturation, we stimulated purified splenic cDCs by CpG in vitro and stained with Abs against costimulatory molecules CD86 and CD80. We found that CpG induced substantial upregulation of CD86 and CD80 at similar levels in both WT and Dlg1-deficient cDCs, demonstrating that Dlg1 did not affect the expression of costimulatory molecules on cDCs including CD8α$^+$ cDCs and CD11b$^+$ cDCs (Supplemental Fig. 2A). For further validation, BMDCs cultured for 9 d were simulated by 100 ng/ml LPS overnight, and an analysis of surface marker expression was performed. Both Dlg1-KO and control BMC produced >80% of BMDCs, which were then gated for the analysis of surface MHC-II, CD80, and CD86 expression. The results showed that expression of CD80, CD86, and MHC-II were similar to that of both WT and Dlg1-KO BMDCs, indicating that the abrogation of Dlg1 did not affect the maturation of BMDCs (Supplemental Fig. 2B, 2C).

Dlg1-KO DCs have lower capacity to mediate Ab responses

The previous results enabled us to check whether Dlg1 deficiency would affect the capacity of DCs to mediate Ab responses. We immunized both *Dlg1*$^{fl/fl}$Cd11c-Cre-GFP and Cd11c-Cre-GFP mice with TI Ag NP–AminoEthylCarboxyMethyl–Ficoll by i.p. injection. Serum NP-specific Ab titers were quantified by ELISA. *Dlg1*$^{fl/fl}$Cd11c-Cre-GFP mice consistently produced lower amounts of NP-specific IgM and IgG Abs than control mice (Fig. 2A). To assess the requirement for Dlg1 expression by cDCs in induction of TD responses, we immunized both *Dlg1*$^{fl/fl}$Cd11c-Cre-GFP and Cd11c-Cre-GFP mice with TD Ag NP_{33}-KLH with CFA by i.p. injection. Sera were collected every 2 wk, and titers of NP-specific Abs were quantified by ELISA. We found a reduction in primary Ab titers in *Dlg1*$^{fl/fl}$Cd11c-Cre-GFP mice when compared with Cd11c-Cre-GFP mice (Fig. 2B–D). Six weeks after primary immunizations, we recalled immunizations with NP_{33}-KLH by i.p. injections. *Dlg1*$^{fl/fl}$Cd11c-Cre-GFP mice produced lesser amounts of IgG and IgM than Cd11c-Cre-GFP control mice (Fig. 2B–D). These results were consistent in both primary and memory Ab responses, and the impaired effects seemed more pronounced in the Ag recall responses. As further validation of the compromised humoral responses in mice with Dlg1 deficiency in cDCs, the generation of germinal center B cells was also impaired in *Dlg1*$^{fl/fl}$Cd11c-Cre-GFP mice (Fig. 2E), which indicated that the deficient Ab responses were induced by

compromised B cell responses as early as germinal center B cell generation. Thus, Dlg1 is required for Ab responses mediated by cDCs in both TI and TD Ag immunizations.

Dlg1 deficiency impairs Ag uptake in DCs

Considering Ag uptake by DCs as the first step in DC-mediated B cell activation and function, we explored the endocytosis of fluorescence-conjugated soluble OVA (OVA-AF647) by cDCs. The results showed that endocytosis of OVA by both $CD8\alpha^+$ cDCs and $CD11b^+$ cDCs was significantly compromised by the loss of Dlg1 (Fig. 3A). We next addressed the potential involvement of Dlg1 in a more specialized function of DCs, namely phagocytosis. Within 1 h of exposure to mouse IgG–coated latex beads (2 μm in diameter), WT BMDCs showed a stronger capacity for phagocytosis at all time points indicated than that of Dlg1-KO BMDCs (Fig. 3B). We also measured BMDC binding of mouse IgG–coated beads in the presence of 10 μM cytochalasin D, which blocks internalization mediated by depolymerizing actin. Most BMDCs had no bound beads at indicated times (Fig. 3C), meaning that impaired Ag responses by DCs were due to impaired uptake or the phagocytosis process but not the initial binding event. Collectively, all these results revealed that Dlg1 would be required for endocytosis and phagocytosis of DCs upon encountering Ags.

Dlg1 deficiency attenuates the production of proinflammatory cytokines by DCs

The ability of DCs to produce proinflammatory cytokines is fundamental for coordinating both innate immune responses and Ab production. Hence, we examined the capacity for producing proinflammatory cytokines including IL-6, TNF-α, and IL-12p40 by DCs in the presence or absence of Dlg1. Our ELISA showed that IL-6, TNF-α, and IL-12p40 were undetectable in both WT and Dlg1-KO BMDC cultures in a quiescent state. WT BMDCs secreted copious amounts of IL-6, TNF-α, and IL-12p40 upon stimulation by CpG or LPS (Fig. 4A). By contrast, Dlg1-KO BMDCs secreted much lower levels of these cytokines (Fig. 4A). Thus, Dlg1 is required for proinflammatory cytokine production by BMDCs in vitro.

To check whether the observations above were also true in vivo, we tested the production of proinflammatory cytokines in *Dlg1*$^{fl/fl}$Cd11c-Cre-GFP mice with LPS-induced septic shock. For this purpose, mice were administrated 1 μg of LPS per mouse by i.v. injection. Sera were collected from *Dlg1*$^{fl/fl}$Cd11c-Cre-GFP and Cd11c-Cre-GFP mice 2 h after LPS challenge. Sera were subjected to ELISA analysis for cytokine production. Consistent with the observation above, production of IL-6, TNF-α, and IL-12p40 in the serum of cDC-specific Dlg1-KO mice was significantly decreased compared with WT control mice (Fig. 4B). To confirm whether LPS would activate WT and Dlg1-KO cDCs in the spleen, we assessed the levels of costimulatory molecule (CD86) expression and found no significant differences from their counterparts (Fig. 4C).

To explore the pathological importance of Dlg1 in DCs, we applied a B16-F10 induced melanoma model, as DCs are routinely found in tumor microenvironments. Proinflammatory cytokines (TNF-α, IL-6, etc.) are known to be highly crucial for supporting tumor growth and providing tumor cells with continuous growth and survival signals (18). As expected, we

consistently found smaller tumor volumes on *Dlg1*$^{fl/fl}$Cd11c-Cre-GFP mice than those on Cd11c-Cre-GFP mice (Fig. 4D). It indicated that Dlg1 was involved in cDC-derived proinflammatory cytokine–mediated tumor formation. All these in vitro and in vivo experiments suggested that loss of Dlg1 impaired the capacity of DCs to produce proinflammatory cytokines.

Dlg1 deficiency does not affect TLR signaling and the transcription of proinflammatory cytokines

We initially proposed that Dlg1 deficiency might impair the transcription of these proinflammatory cytokines, which led to their aforementioned reduced protein production. To examine our hypothesis, we quantified the related mRNA expression of different cytokines in BMDCs. Unexpectedly, Dlg1-KO BMDCs produced similar amount of IL-6, TNF-α, and IL-12p40 at the mRNA level compared with WT BMDCs (Supplemental Fig. 3A). To further validate these observations, we quantified TLR4 expression on splenic cDCs. We found that TLR4 was expressed evenly across all DC subtypes (Supplemental Fig. 3B). Then we examined activation of NF-κB transcription factors upon LPS stimulation. The results showed that IκBα degradation in Dlg1-KO BMDCs showed similar kinetics to those of WT BDMCs (Supplemental Fig. 3C). LPS-induced phosphorylation of JNK and other signaling downstream of TLR4 in Dlg1-KO BMDCs was also relatively comparable to that of control BDMCs (Supplemental Fig. 3C). Phosphorylations of AKT were also similar in the presence or absence of Dlg1 (Supplemental Fig. 3D). It implied that the TLR signaling pathway was not altered by Dlg1. Collectively, these results indicated that Dlg1 did not affect the transcription of the proinflammatory cytokines.

Dlg1 modulates DC activation and function through voltage-gated K^+ channels

To identify target molecules responsible for compromised functions of DCs upon Dlg1 deficiency, we examined total protein levels in CD11b$^+$ cDCs from *Dlg1*$^{fl/fl}$Cd11c-Cre-GFP and Cd11c-Cre-GFP mice MS-supported quantitative proteomics analyses. We identified 292 downregulated proteins and 602 upregulated proteins upon Dlg1 depletion in cDCs (Supplemental Fig. 4A). When these differentially expressed proteins were subjected to GO term enrichment analysis, we found that genes related to transport biological process (BP) were mainly affected in the absence of Dlg1 (Fig. 5A, Supplemental Fig. 4B, 4C). Of these transport BP–related proteins, Atp5l (ATP synthase subunit g, mitochondrial) and Kcnab1 (voltage-gated potassium channel subunit β-1, Kvβ1) showed top differences in Dlg1-KO CD11b$^+$ cDCs (Fig. 5B). In fact, Atp5l is one subunit of the F_0ATPase complex, which was reported to support ATP transporting (19). Meanwhile, MS analyses also showed a mildly lower Kcnab2 (voltage-gated potassium channel subunit β-2, Kvβ2) expression in Dlg1-KO CD11b$^+$ cDCs (Supplemental Fig. 4D). It demonstrated that Dlg1 may be required for Kvβ subunit expression in cDCs. To validate these results from MS, we used anti–pan-Kvβ subunit Ab to perform immunoblots and readily confirmed the reduced expression level of voltage-gated K^+ channel subunits in both CD8α$^+$ cDCs and CD11b$^+$ cDCs, as well as in BMDCs upon Dlg1 deficiency (Fig. 5C, 5D, Supplemental Fig. 4E). Ag-induced activation and cytokine secretion processes have been reported to be impaired in voltage-gated K^+ channel–deficient T cells (20–22). We then focused on voltage-gated K^+ channel family members in the following studies.

To check directly whether the functions of ion channels were affected in DCs upon Dlg1 deficiency, we performed whole-cell voltage clamp experiments. To obtain current–voltage curves, WT BMDCs were held at a holding potential of −80 mV, and whole-cell currents were measured by 200-ms square wave voltage pulses from −80 to +60 mV in 10-mV steps delivered at 20 ms intervals (Fig. 6A). Strikingly, the currents were significantly decreased by pretreatment of a nonspecific voltage-gated K^+ channel inhibitor, 4-aminopyridine (Fig. 6B), mirroring the proteomic results above. Consistently, in the Dlg1-KO group, K^+ current amplitudes evoked by depolarization pulses from −30 to +60 mV were significantly reduced as compared with the WT (Fig. 6C–E), which agreed with a role of Dlg1 in the function of certain K^+ channels. Dlg1 is known to interact with the C-terminal domain of Kv1.3 through PDZ binding domain (23, 24). Importantly, Dlg family members were reported to protect Kv1.3 against its endocytosis and ubiquitination and thus maintain the plasma membrane localization and function of Kv1.3 (25). Moreover, both Kvβ1 and Kvβ2 β-subunits, as identified in the aforementioned quantitative proteomics analysis, were reported to interact with Kv1 α-subunits, and Kvβ, when coexpressed with Kv1.3, drastically increased K^+ current amplitudes in human T cells (26, 27). Additionally, there are published studies showing that Kv1.3 and Kv1.5 channels were expressed on human blood-derived DCs (28). Based on all these messages, we tested the Kv1.3 and Kv 1.5 channel expression levels in BMDCs upon Dlg1 KO. Western blotting showed that WT mouse-derived BMDCs expressed the Kv1.3 (Fig. 6F) but not the Kv1.5 channel (Fig. 6G). Interestingly, the expression of Kv1.3 was significantly downregulated in Dlg1-KO BMDCs (Fig. 6F), although the mRNA of Kv1.3 was not affected in Dlg1-KO BMDCs (Fig. 6H). Further, the amplitudes of K^+ current were significantly inhibited with the addition of 5 μm PAP-1, a Kv1.3 selective inhibitor (Fig. 6I). These results suggested that Dlg1 is indispensable for maintaining the plasma membrane location and function of voltage-gated K^+ channels in DCs. Because Kv1.3 is involved in K^+ flux and linked to the downstream Ca^{2+} flux event (29), we performed the Ca^{2+} flux experiment to investigate the function of the Kv1.3 channel in DC activation. It was evident that Ca^{2+} flux was much stronger in WT BMDCs compared with that of Dlg1-KO BMDCs upon LPS stimulation (Fig. 6J).

To directly examine the importance of the Kv1.3 channel in DC function, we used PAP-1, a Kv1.3 selective inhibitor, to pretreat both WT and Dlg1-KO BMDCs before assessing their phagocytosis and cytokine secretion capabilities. We found that in the presence of PAP-1, the phagocytosis capacity of WT BMDCs was impaired as expected (Fig. 7A). In contrast, Kv1.3 channel inhibitor did not further decrease the phagocytosis function of Dlg1-KO BMDCs, suggesting that Dlg1 plays an important role in the phagocytosis process of DCs in a Kv1.3-dependent manner. Similarly, PAP-1 blocked the production of proinflammatory cytokines in both WT and Dlg1-KO BMDCs, the effect of which is more drastic in WT BMDCs than in Dlg1-KO BMDCs (Fig. 7B). Ca^{2+} flux in WT BMDCs was impaired in presence of PAP-1 (Fig. 7C), suggesting that Dlg1 plays an important role in TLR activation–induced Ca^{2+} flux and cytokine production of DCs in a Kv1.3-dependent manner.

Consequently, this study illustrated that Dlg1 played an important role in DC functions by maintaining the integrity of voltage-gated K^+ channels. As a consequence, Dlg1 deficiency drastically impaired DC functions, consistent with the published studies showing that Kv1.3

deficiency led to a suppressed function in different types of cells, including DCs, T cells, microglia, and glioma (20, 30–32).

Discussion

DCs represent an essential component in innate responses and subsequent adaptive immunity through Ag presentation to lymphocytes and secretion of proinflammatory cytokines. During cell–cell contacts, DCs form immunological synapses on plasma membranes, promoting conjugations with B cells or T cells (3–5). Dlg1 is a critical component of the Scribble complex, which plays an important role in the function of immunological synapses (6, 9). However, the function of Dlg1 in DCs remains unclear. In this study, by taking advantage of mice with conditional KO of Dlg1 in cDCs, we found that Dlg1 was indispensable for DC activation and function. Dlg1-KO DCs showed a lower capacity in both TI and TD Ab responses. Further studies showed that Dlg1-KO DCs had decreased Ag uptake by endocytosis and phagocytosis. Thus, an explanation for the weaker Ab responses in Dlg1-KO DC mice may be that Dlg1 deficiency in DCs compromised the endocytosis and phagocytosis capacity of DCs, leading to restricted B cell activation and proliferation. In addition to capturing and presenting Ags, DCs can also produce proinflammatory cytokines to regulate innate and adaptive immune responses. Upon LPS stimulation, the level of cytokines secreted by Dlg1-KO BMDCs was significantly lower than that of WT BMDCs, whereas TLR signaling and the transcription of proinflammatory cytokines were not affected. This meant that Dlg1 was responsible for cytokine translation other than induction or transcription.

We further investigated the molecular mechanism through which Dlg1 is involved in DC functions. Previous studies reported that voltage-gated K^+ channels expressed on DCs played a critical role in DC activation and functions (28, 30, 33). Colocalization between Kv1.3 and Dlg1 in the immunological synapse was previously reported in T cells (29). Our data showed that loss of Dlg1 decreased the amount of Kv1.3 channel protein in DCs. These results are consistent with previous studies that arduously investigated the regulation of Kv1.3 by Dlg family members in some other types of cells, including T cells (23, 25, 34). In those cells, Dlg family members interacted with Kv1.3 channel protein and recruited Kv1.3 channel protein into the immunological synapse, protecting Kv1.3 channel protein from degradation. Kv1.3 has also been reported to interact with Dlg1 through its C terminus (24). Furthermore, cell biological studies indicated that the interaction between Dlg1 and K^+ channels occurs at a very early biosynthetic pathway of these channel proteins when they are in the endoplasmic reticulum (35), suggesting a critical role of Dlg1 in the packaging and trafficking of K^+ channels. As a consequence, in the patch-clamp experiments, decreased current amplitude was observed following treatment with different voltages in Dlg1-KO BMDCs. This observation was consistent with previous studies showing that synaptic clustering of Shaker-type K^+ channels was abolished by loss-of-function mutations in *dlg* in *Drosophila* (24). In addition to clustering the Shaker-type K^+ channels, Dlg1 or PSD-95 also increased the whole-cell Kir4.1 current magnitude in glial cells, indicating that Dlg1 and PSD-95 might regulate the activity of the Kir4.1 channel, which is an inwardly rectifying K^+ channel (36). Thus, all these results are in line with our studies showing that Dlg1 is important for the function of voltage-gated K^+ channels.

Moreover, voltage-gated K^+ channels are known to be important for subsequent IL-6 and TNF-α production in BMDCs (30, 33, 37). Accordingly, our results showed that Dlg1 deficiency decreased the level of voltage-gated K^+ channels in BMDCs, leading to significantly impaired IL-6 and TNF-α production. These results are also consistent with published studies showing that Kv1.3 deficiency leads to a suppressed function in different types of immune cells, including T cells, microglia, and glioma (20, 31, 32). In contrast, the increased Kv1.3 expression resulted in elevated K^+ flux and T cell hyperactivation (22). In addition, K^+ channel activity and cell membrane potential are also thought to provide the necessary electrical driving force to regulate Ca^{2+} flux by maintaining negative membrane potential in BMDCs (30). The results in this report further showed that Dlg1 regulates Ca^{2+} signaling in BMDCs by regulating Kv1.3 channel protein expression, consistent with reported studies in T cells (22, 29). However, our data also showed that Dlg1 deficiency does not affect IL-12p40 production in BMDCs; thus, the exact role of K^+ channels in DC function still needs to be further investigated.

Therefore, this study provided, to our knowledge, a novel insight into Dlg1 and the voltage-gated K^+ channel axis in DC functions by maintaining the Ags endocytosis and phagocytosis, the proinflammatory cytokine production in both innate and adaptive immune responses. In conclusion, Dlg1 and voltage-gated K^+ channels in DCs are emerging as possible targets for therapeutic manipulation of excessive proinflammatory cytokines. The therapeutic promise remains to be further realized, but the future does look encouraging.

Supplementary Material

Refer to Web version on PubMed Central for supplementary material.

Acknowledgments

We thank Dr. Susan K. Pierce (National Institute of Allergy and Infectious Diseases, National Institutes of Health) for generously providing experimental materials. We also thank Dr. Haiteng Deng (Tsinghua University) for providing quantitative proteomics services.

This work was supported by funds from the National Natural Science Foundation of China (81825010, 81730043, 81621002, and 31811540397). L. Wu is supported by the National Natural Science Foundation of China (31330027 and 91642207) and a National Key Basic Research Grant from the Ministry of Science and Technology of China (2015CB943200). This work was also supported by the National Multiple Sclerosis Society (Career Transition Award TA 30 59 -A-2 to C.W.).

Abbreviations used in this article:

AF647	Alexa Fluor 647
BMC	bone marrow cell
BMDC	bone marrow–derived DC
BP	biological process
cDC	conventional DC
DC	dendritic cell

Dlg	discs large
Dlg1	discs large homologue 1
GO	gene ontology
KO	knockout
MHC-II	MHC class II
MS	mass spectrometry
NP	4-hydroxy-3-nitrophenylacetic
NP_{33}-KLH	4-hydroxy-3-nitrophenylacetyl 33–keyhole limpet hemocyanin
pDC	plasmacytoid DC
TD	thymus-dependent
TI	thymus-independent
WT	wild-type

References

1. Banchereau J, and Steinman RM. 1998. Dendritic cells and the control of immunity. Nature 392: 245–252. [PubMed: 9521319]
2. Shortman K, and Liu YJ. 2002. Mouse and human dendritic cell subtypes. Nat. Rev. Immunol 2: 151–161. [PubMed: 11913066]
3. Verboogen DR, Dingjan I, Revelo NH, Visser LJ, ter Beest M, and van den Bogaart G. 2016. The dendritic cell side of the immunological synapse. Biomol. Concepts 7: 17–28. [PubMed: 26741354]
4. Benvenuti F 2016. The dendritic cell synapse: a life dedicated to T cell activation. Front. Immunol 7: 70. [PubMed: 27014259]
5. Qi H, Egen JG, Huang AY, and Germain RN. 2006. Extrafollicular activation of lymph node B cells by antigen-bearing dendritic cells. Science 312: 1672–1676. [PubMed: 16778060]
6. Ludford-Menting MJ, Oliaro J, Sacirbegovic F, Cheah ETY, Pedersen N, Thomas SJ, Pasam A, Iazzolino R, Dow LE, Waterhouse NJ, et al. 2005. A network of PDZ-containing proteins regulates T cell polarity and morphology during migration and immunological synapse formation. Immunity 22: 737–748. [PubMed: 15963788]
7. Caria S, Magtoto CM, Samiei T, Portela M, Lim KYB, How JY, Stewart BZ, Humbert PO, Richardson HE, and Kvansakul M. 2018. *Drosophila melanogaster* Guk-holder interacts with the Scribbled PDZ1 domain and regulates epithelial development with Scribbled and Discs Large. J. Biol. Chem 293: 4519–4531. [PubMed: 29378849]
8. Roche JP, Packard MC, Moeckel-Cole S, and Budnik V. 2002. Regulation of synaptic plasticity and synaptic vesicle dynamics by the PDZ protein Scribble. J. Neurosci 22: 6471–6479. [PubMed: 12151526]
9. Liu W, Chen E, Zhao XW, Wan ZP, Gao YR, Davey A, Huang E, Zhang L, Crocetti J, Sandoval G, et al. 2012. The scaffolding protein synapse-associated protein 97 is required for enhanced signaling through isotype-switched IgG memory B cell receptors. Sci. Signal 5: ra54. [PubMed: 22855505]
10. Oliva C, Escobedo P, Astorga C, Molina C, and Sierralta J. 2012. Role of the MAGUK protein family in synapse formation and function. Dev. Neurobiol 72: 57–72. [PubMed: 21739617]
11. Kim E, and Sheng M. 2004. PDZ domain proteins of synapses. Nat. Rev. Neurosci 5: 771–781. [PubMed: 15378037]

12. Sandoval GJ, Graham DB, Gmyrek GB, Akilesh HM, Fujikawa K, Sammut B, Bhattacharya D, Srivatsan S, Kim A, Shaw AS, et al. 2013. Novel mechanism of tumor suppression by polarity gene discs large 1 (DLG1) revealed in a murine model of pediatric B-ALL. Cancer Immunol. Res 1: 426–437. [PubMed: 24778134]
13. Round JL, Humphries LA, Tomassian T, Mittelstadt P, Zhang M, and Miceli MC. 2007. Scaffold protein Dlgh1 coordinates alternative p38 kinase activation, directing T cell receptor signals toward NFAT but not NF-kappaB transcription factors. Nat. Immunol 8: 154–161. [PubMed: 17187070]
14. Barreda D, Sánchez-Galindo M, López-Flores J, Nava-Castro KE, Bobadilla K, Salgado-Aguayo A, and Santos-Mendoza T. 2018. PDZ proteins are expressed and regulated in antigen-presenting cells and are targets of influenza A virus. J. Leukoc. Biol 103: 731–738. [PubMed: 29345359]
15. Vremec D, and Segura E. 2013. The purification of large numbers of antigen presenting dendritic cells from mouse spleen. Methods Mol. Biol 960: 327–350. [PubMed: 23329497]
16. Guo X, Wu N, Shang Y, Liu X, Wu T, Zhou Y, Liu X, Huang J, Liao X, and Wu L. 2017. The novel toll-like receptor 2 agonist SUP3 enhances antigen presentation and T cell activation by dendritic cells. Front. Immunol 8: 158. [PubMed: 28270814]
17. Qu H, Chen Y, Cao G, Liu C, Xu J, Deng H, and Zhang Z. 2016. Identification and validation of differentially expressed proteins in epithelial ovarian cancers using quantitative proteomics. Oncotarget 7: 83187–83199. [PubMed: 27825122]
18. Grivennikov SI, Greten FR, and Karin M. 2010. Immunity, inflammation, and cancer. Cell 140: 883–899. [PubMed: 20303878]
19. Zhdanov AV, Andreev DE, Baranov PV, and Papkovsky DB. 2017. Low energy costs of F1Fo ATP synthase reversal in colon carcinoma cells deficient in mitochondrial complex IV. Free Radic. Biol. Med 106: 184–195. [PubMed: 28189850]
20. Gocke AR, Lebson LA, Grishkan IV, Hu L, Nguyen HM, Whartenby KA, Chandy KG, and Calabresi PA. 2012. Kv1.3 deletion biases T cells toward an immunoregulatory phenotype and renders mice resistant to autoimmune encephalomyelitis. J. Immunol 188: 5877–5886. [PubMed: 22581856]
21. Liu QH, Fleischmann BK, Hondowicz B, Maier CC, Turka LA, Yui K, Kotlikoff MI, Wells AD, and Freedman BD. 2002. Modulation of Kv channel expression and function by TCR and costimulatory signals during peripheral CD4(+) lymphocyte differentiation. J. Exp. Med 196: 897–909. [PubMed: 12370252]
22. Kang JA, Park SH, Jeong SP, Han MH, Lee CR, Lee KM, Kim N, Song MR, Choi M, Ye M, et al. 2016. Epigenetic regulation of Kcna3-encoding Kv1.3 potassium channel by cereblon contributes to regulation of CD4+ T-cell activation. Proc. Natl. Acad. Sci. USA 113: 8771–8776. [PubMed: 27439875]
23. Szilágyi O, Boratkó A, Panyi G, and Hajdu P. 2013. The role of PSD-95 in the rearrangement of Kv1.3 channels to the immunological synapse. Pflugers Arch. 465: 1341–1353. [PubMed: 23553419]
24. Tejedor FJ, Bokhari A, Rogero O, Gorczyca M, Zhang J, Kim E, Sheng M, and Budnik V. 1997. Essential role for dlg in synaptic clustering of Shaker K+ channels in vivo. J. Neurosci 17: 152–159. [PubMed: 8987744]
25. Martínez-Mármol R, Styrczewska K, Pérez-Verdaguer M, Vallejo-Gracia A, Comes N, Sorkin A, and Felipe A. 2017. Ubiquitination mediates Kv1.3 endocytosis as a mechanism for protein kinase C-dependent modulation. Sci. Rep 7: 42395. [PubMed: 28186199]
26. McCormack T, McCormack K, Nadal MS, Vieira E, Ozaita A, and Rudy B. 1999. The effects of Shaker beta-subunits on the human lymphocyte K+ channel Kv1.3. J. Biol. Chem 274: 20123–20126. [PubMed: 10400624]
27. Nakahira K, Shi G, Rhodes KJ, and Trimmer JS. 1996. Selective interaction of voltage-gated K+ channel beta-subunits with alpha-subunits. J. Biol. Chem 271: 7084–7089. [PubMed: 8636142]
28. Mullen KM, Rozycka M, Rus H, Hu L, Cudrici C, Zafranskaia E, Pennington MW, Johns DC, Judge SI, and Calabresi PA. 2006. Potassium channels Kv1.3 and Kv1.5 are expressed on blood-derived dendritic cells in the central nervous system. Ann. Neurol 60: 118–127. [PubMed: 16729292]

29. Beeton C, Wulff H, Standifer NE, Azam P, Mullen KM, Pennington MW, Kolski-Andreaco A, Wei E, Grino A, Counts DR, et al. 2006. Kv1.3 channels are a therapeutic target for T cell-mediated autoimmune diseases. Proc. Natl. Acad. Sci. USA 103: 17414–17419. [PubMed: 17088564]

30. Matzner N, Zemtsova IM, Nguyen TX, Duszenko M, Shumilina E, and Lang F. 2008. Ion channels modulating mouse dendritic cell functions. J. Immunol 181: 6803–6809. [PubMed: 18981098]

31. Rangaraju S, Raza SA, Pennati A, Deng Q, Dammer EB, Duong D, Pennington MW, Tansey MG, Lah JJ, Betarbet R, et al. 2017. A systems pharmacology-based approach to identify novel Kv1.3 channel-dependent mechanisms in microglial activation. J. Neuroinflammation 14: 128. [PubMed: 28651603]

32. Grimaldi A, D'Alessandro G, Di Castro MA, Lauro C, Singh V, Pagani F, Sforna L, Grassi F, Di Angelantonio S, Catacuzzeno L, et al. 2018. Kv1.3 activity perturbs the homeostatic properties of astrocytes in glioma. Sci. Rep 8: 7654. [PubMed: 29769580]

33. Tyan L, Sopjani M, Dërmaku-Sopjani M, Schmid E, Yang W, Xuan NT, Shumilina E, and Lang F. 2010. Inhibition of voltage-gated K+ channels in dendritic cells by rapamycin. Am. J. Physiol. Cell Physiol 299: C1379–C1385. [PubMed: 20926775]

34. Kuras Z, Kucher V, Gordon SM, Neumeier L, Chimote AA, Filipovich AH, and Conforti L. 2012. Modulation of Kv1.3 channels by protein kinase A I in T lymphocytes is mediated by the disc large 1-tyrosine kinase Lck complex. Am. J. Physiol. Cell Physiol 302: C1504–C1512. [PubMed: 22378744]

35. Gardoni F, Mauceri D, Marcello E, Sala C, Di Luca M, and Jeromin A. 2007. SAP97 directs the localization of Kv4.2 to spines in hippocampal neurons: regulation by CaMKII. J. Biol. Chem 282: 28691–28699. [PubMed: 17635915]

36. Horio Y, Hibino H, Inanobe A, Yamada M, Ishii M, Tada Y, Satoh E, Hata Y, Takai Y, and Kurachi Y. 1997. Clustering and enhanced activity of an inwardly rectifying potassium channel, Kir4.1, by an anchoring protein, PSD-95/SAP90. J. Biol. Chem 272: 12885–12888. [PubMed: 9148889]

37. Shumilina E, Zahir N, Xuan NT, and Lang F. 2007. Phosphoinositide 3-kinase dependent regulation of Kv channels in dendritic cells. Cell. Physiol. Biochem 20: 801–808. [PubMed: 17982262]

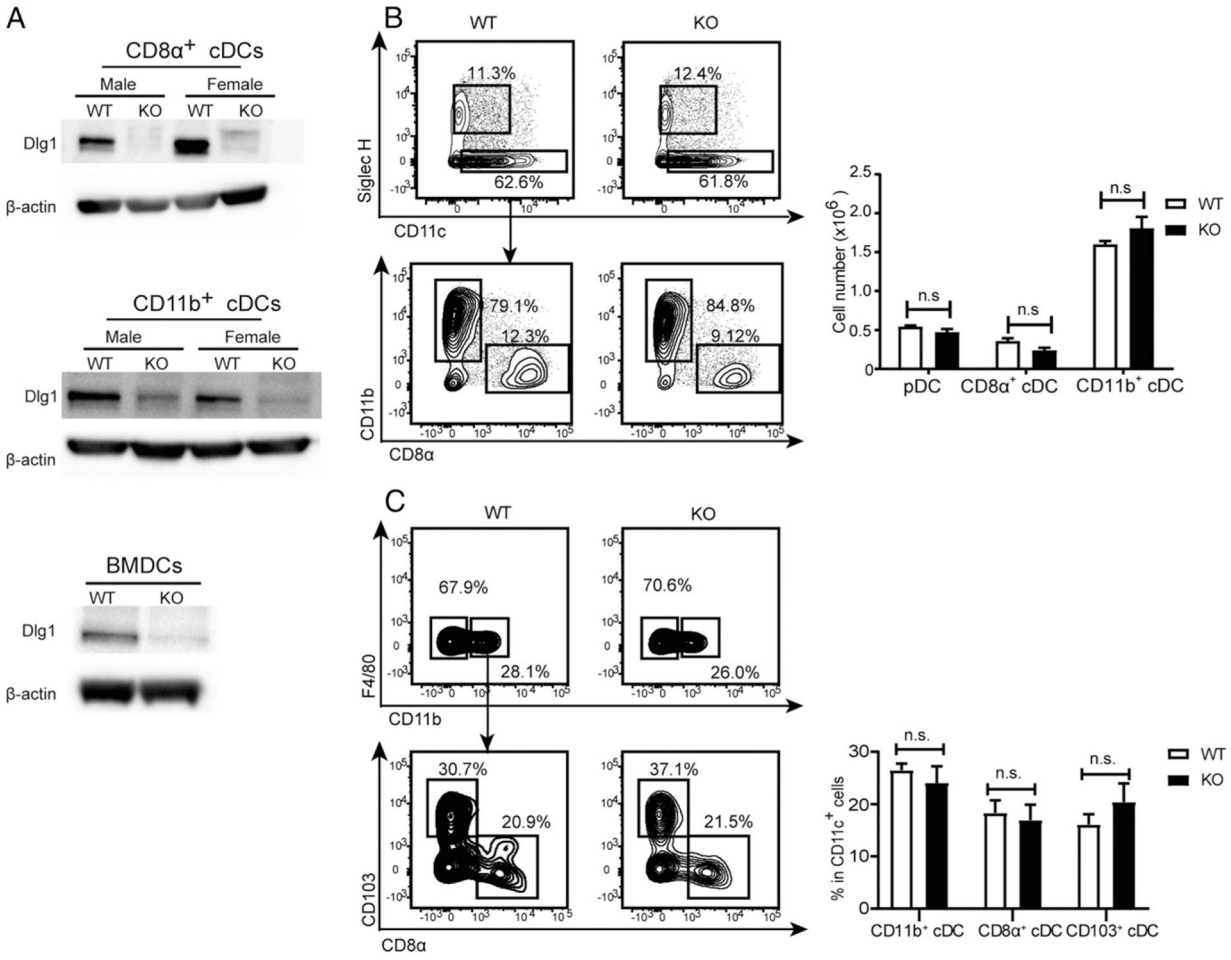

FIGURE 1.

Dlg1 is not essential for DC development. (**A**) Splenic cDCs ($CD11c^+CD8\alpha^+$ or $CD11c^+CD11b^+$) and $CD11c^+$ BMDCs were purified, and protein expression of Dlg1 was analyzed by Western blot analysis with β-actin as loading control. Data are representative of at least two independent experiments. (**B** and **C**) DCs from spleens (B) and lymph nodes (C) were analyzed by flow cytometry for comparison between WT (Cd11c-Cre-GFP) and Dlg1-KO (*Dlg1*$^{fl/fl}$Cd11c-Cre-GFP) mice, respectively. Total cell numbers or percentages of DC subsets were analyzed. Data are representative of at least two independent experiments (four mice in each group). n.s., not significant.

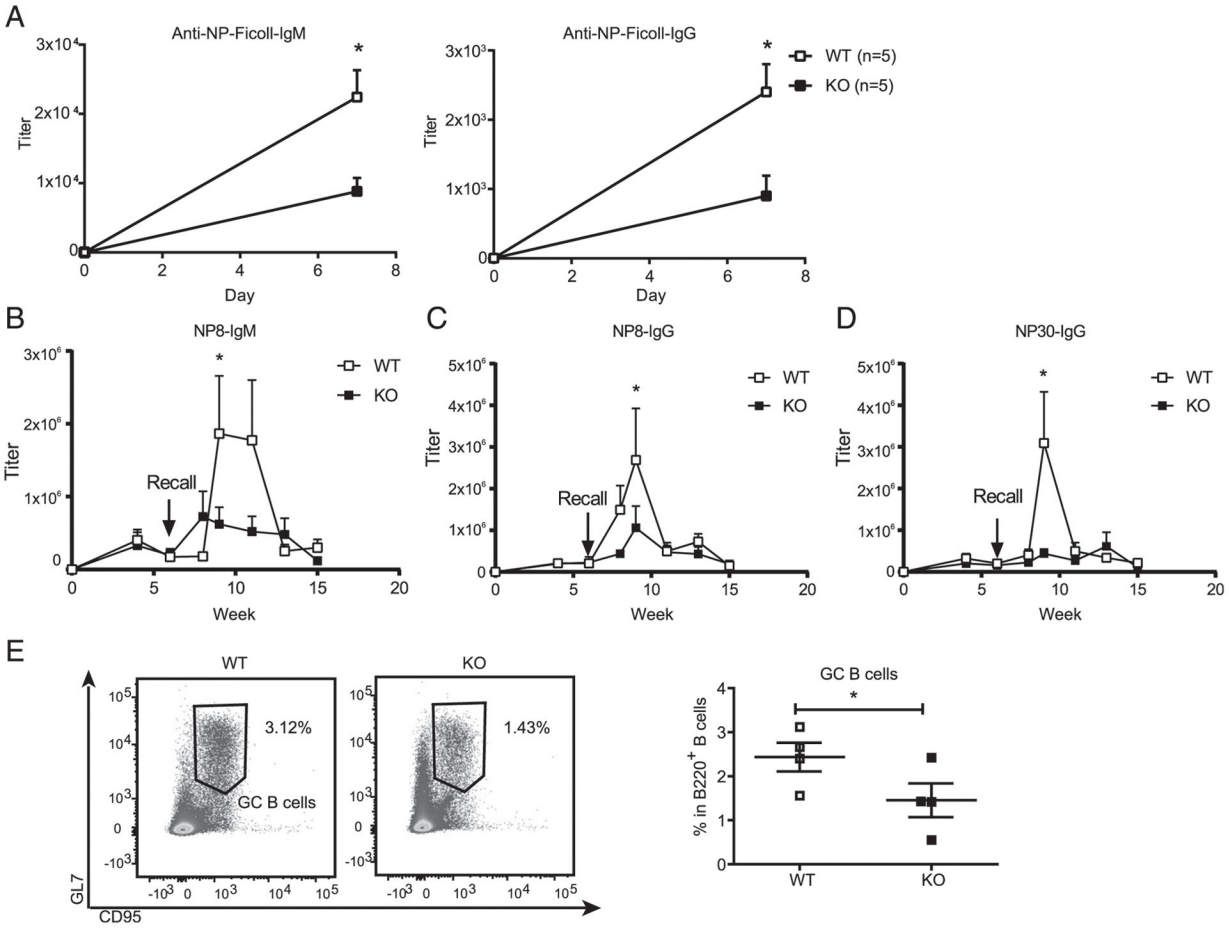

FIGURE 2.

Dlg1-KO DCs are deficient in promoting Ab responses. (**A**) IgM and IgG response to TI Ag. WT (Cd11c-Cre-GFP) and KO (*Dlg1*$^{fl/fl}$Cd11c-Cre-GFP) mice were immunized by TI Ag NP-Ficoll by i.p. injection. Serum IgM and IgG specific to NP-Ficoll at day 7 were measured in WT (Cd11c-Cre-GFP) and KO (*Dlg1*$^{fl/fl}$Cd11c-Cre-GFP) mice by ELISA (*n* indicates the number of mice in each group). Titers were defined as the maximum serum dilution. Data are representative of two independent experiments. (**B**–**D**) Kinetics of IgM and IgG responses to TD Ags. WT (Cd11c-Cre-GFP) and KO (*Dlg1*$^{fl/fl}$Cd11c-Cre-GFP) mice were immunized on day 0 by TD Ag NP_{33}-KLH with CFA as adjuvant. Serum IgM (nitrophenyl 8mer-captured [NP8-IgM]), high affinity IgG (NP8-IgG), and total IgG (NP30-IgG) were examined by ELISA. Titers were defined as the maximum serum dilution. Data were pooled from two independent experiments (WT = 7 mice, KO = 6 mice, one-tailed). (**E**) Representative flow cytometric graph (left) and quantification of germinal center B cells ($B220^+CD95^+GL7^+$) (right). Spleens were collected from WT (Cd11c-Cre-GFP) and KO (*Dlg1*$^{fl/fl}$Cd11c-Cre-GFP) mice 7 d post-immunization with sheep RBCs. Data were pooled from four mice per phenotype group (one-tailed). *$p < 0.05$.

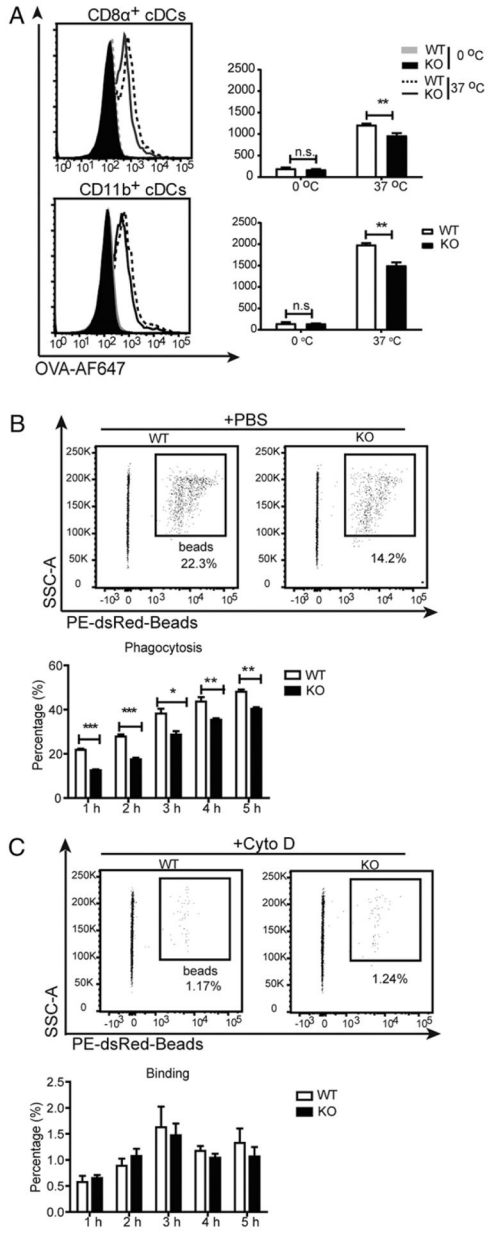

FIGURE 3.

Dlg1 deficiency impairs the capacity of Ag uptake by DCs. (**A**) Ag uptake by WT or Dlg1-KO splenic cDCs. Purified splenic cDCs were incubated with AF647-OVA at 0 or 37°C for 30 min. After washing with cold PBS, cells were measured for median fluorescence intensity (MFI) of AF647. Representative data from three independent experiments were shown (one mouse per genotype assayed in at least triplicate wells). (**B** and **C**) Representative flow cytometric graphs (upper panels) and quantification (bottom panels) of phagocytosis of WT and Dlg1-KO BMDCs. BMDCs were incubated with IgG-coated latex beads in the absence (B) or presence of 10 μM cytochalasin D (C). Percentages were calculated by the phagocytosed $CD11c^+$ BMDCs in $CD11c^+$ BMDCs. Data are

representative of two independent experiments (one mouse per genotype assayed in quadruplicate wells). *$p < 0.05$, **$p < 0.01$, ***$p < 0.001$. n.s., not significant.

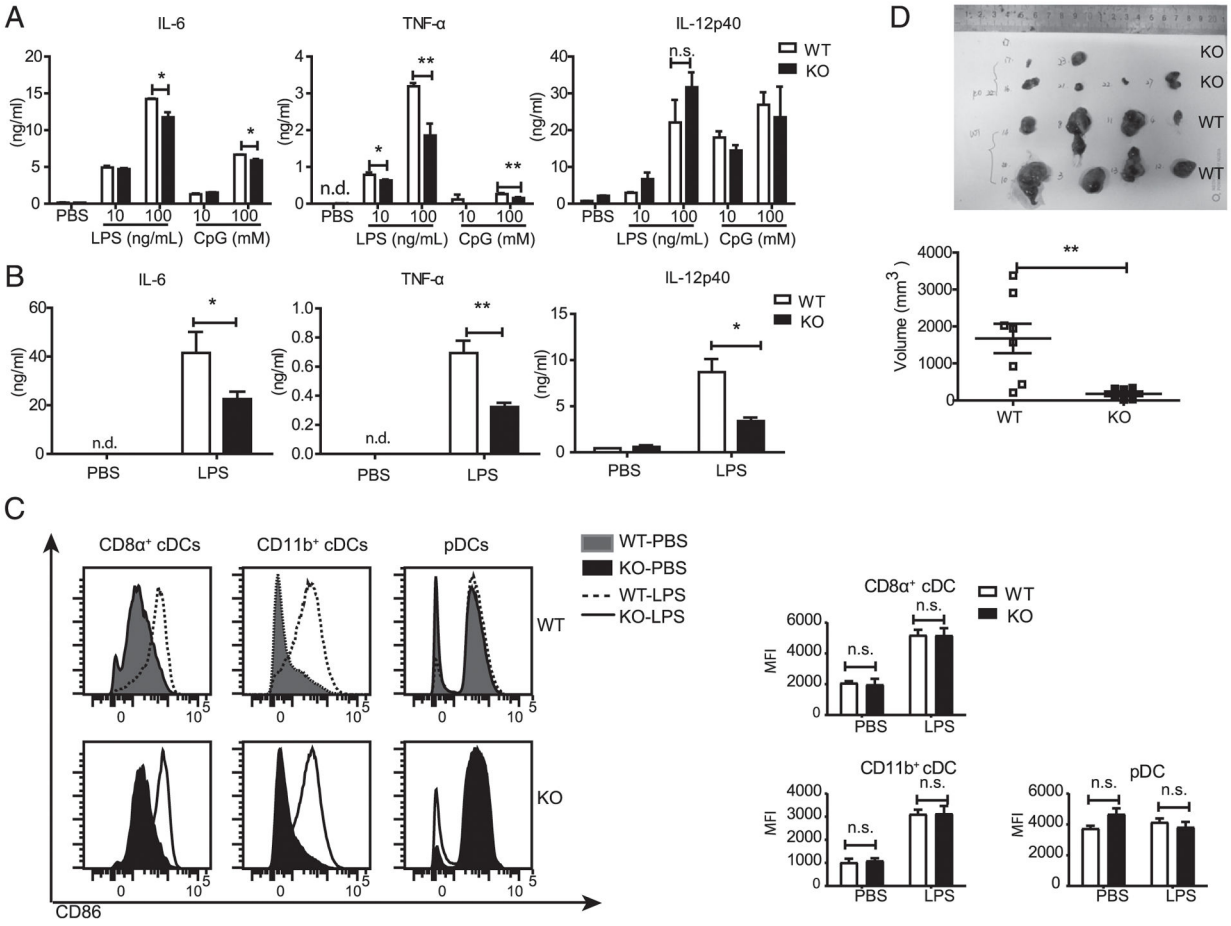

FIGURE 4.

Dlg1 deficiency attenuates the capacity of DCs to produce proinflammatory cytokines. (**A**) IL-6, TNF-α, and IL-12p40 production by BMDCs from WT (Cd11c-Cre-GFP) mice and KO (*Dlg1*$^{fl/fl}$Cd11c-Cre-GFP) mice upon stimulation with indicated concentrations of LPS and CpG for 6 h. Data are pooled from three mice assayed in triplicate wells. (**B**) IL-6, TNF-α, and IL-12p40 concentrations in mice serum. WT (Cd11c-Cre-GFP) mice and KO (*Dlg1*$^{fl/fl}$Cd11c-Cre-GFP) mice were i.v. injected with LPS (1 μg/mouse) for 2 h. Then, serum was collected, and cytokine production was determined by ELISA. Data are representative of two experiments (two to four mice in each group). (**C**) Expression of surface costimulatorory molecules on splenic cDCs from the mice in (B). Data are representative of two experiments. (**D**) Tumor growth of B16-F10 melanoma cells in *Dlg1*$^{fl/fl}$Cd11c-Cre-GFP mice and Cd11c-Cre-GFP mice. Mice were s.c. injected with B16-F10 melanoma cells (5×10^5 cells per mouse), and tumor sizes were measured 10 d postinjection. Pooled data from WT mice ($n = 8$) and KO mice ($n = 6$) were presented. *$p <$ 0.05, **$p < 0.01$. n.d., not detected; n.s., not significant.

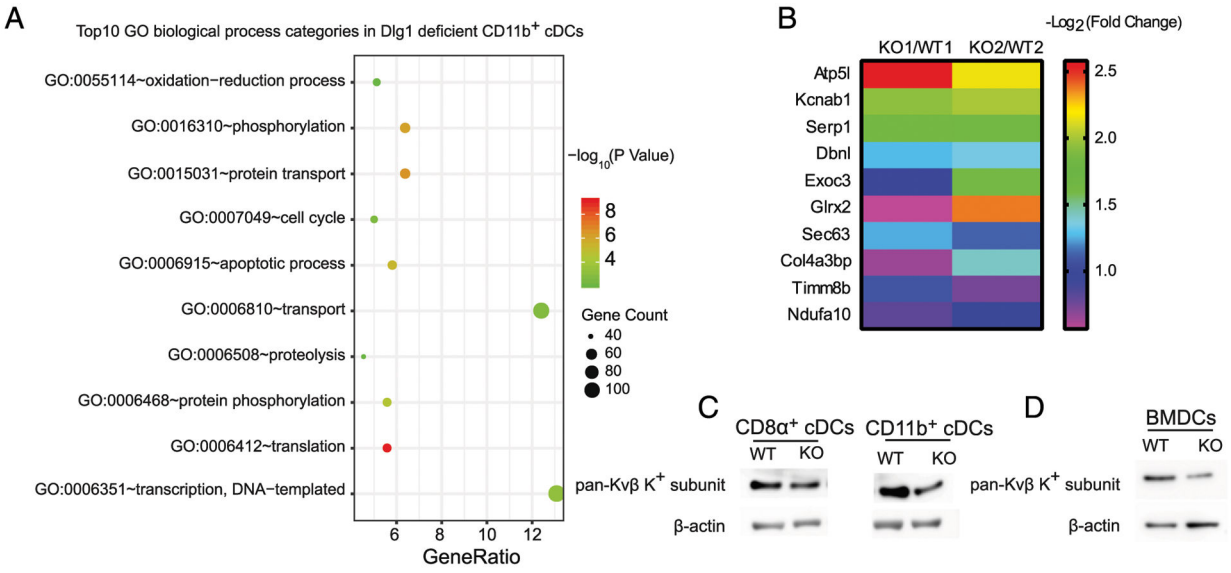

FIGURE 5.

Dlg1 deficiency does not affect TLR signaling and the transcription of proinflammatory cytokines. (**A**) Top 10 GO BP categories in identified proteins (both upregulated and downregulated proteins). Plot colors represent the statistical significance. GeneRatio (%) represents the proportion of genes in total genes. Plot sizes represent the identified protein numbers in MS. (**B**) Top 10 downregulated proteins in the transport BP group from Dlg1-KO CD11b^{+} cDCs. The 10 downregulated proteins were identified from MS data. Each group (KO/WT) indicated one pair of *Dlg1*$^{fl/fl}$Cd11c-Cre-GFP and Cd11c-Cre-GFP mice. Color bar represents protein fold change. (**C** and **D**) Expression levels of pan-Kvβ K^{+} subunit in DCs from *Dlg1*$^{fl/fl}$Cd11c-Cre-GFP mice and Cd11c-Cre-GFP mice, respectively. Whole-cell lysate samples of WT and Dlg1-KO DC subsets were subjected to Western blotting as indicated and probed with anti–pan-Kvβ subunit primary Ab. Loading controls (β-actin) were derived from the same samples. Splenic cDCs (CD11c^{+}CD8α^{+} or CD11c^{+}CD11b^{+}) in (C) and BMDCs (CD11c^{+}) in (D) are shown. Data are representative of three independent experiments.

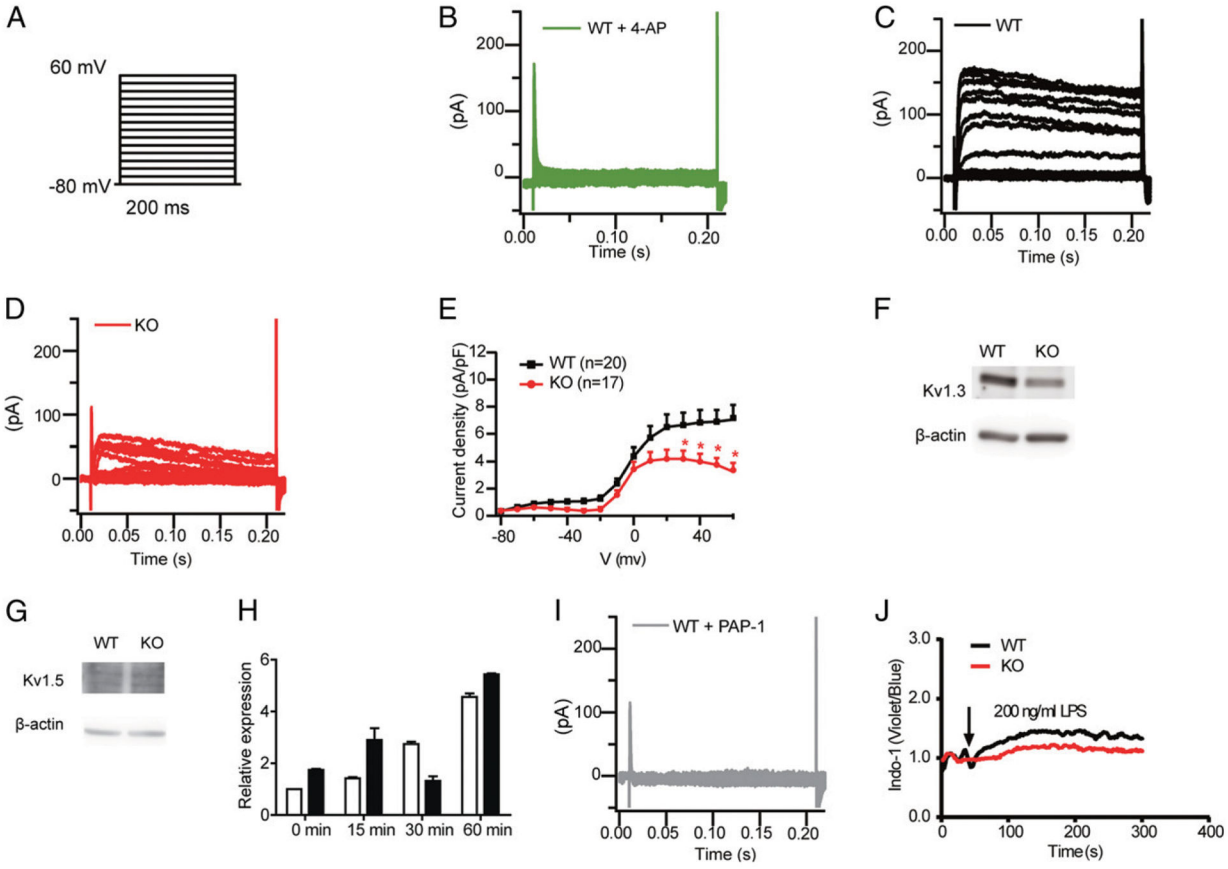

FIGURE 6.

Dlg1 modulates DC activation through the Kv1.3 channel. (**A**) The voltage protocol is shown (not to scale), whereby cells were held at −80 mV, and voltage steps were applied in +10-mV increments for 200 ms from −80 to +60 mV. (**B**) Representative voltage-gated currents recorded from WT BMDCs incubated with 4-aminopyridine (4-AP; 10 μM). (**C**) Representative voltage-gated currents recorded from WT BMDCs. (**D**) Representative voltage-gated currents recorded from Dlg1-KO BMDCs. (**E**) Mean current-voltage curve relationships (n = 17–20 cells) of Kv^+ currents in BMDCs. BMDCs were identified by GFP^+ under confocal microscopy. Data were pooled from four mice in each group. *$p < 0.05$. (**F** and **G**) Expression of Kv1.3 and Kv1.5 in WT and Dlg1-KO BMDCs. BMDCs from WT (Cd11c-Cre-GFP) and KO (*Dlg1*$^{fl/fl}$Cd11c-Cre-GFP) mice were purified as $CD11c^+$ cells. Whole-cell lysis samples of purified $CD11c^+$ WT and Dlg1-KO BMDCs were subjected to Western blot analysis and probed with specific Abs as indicated. Data are representative of at least three independent experiments. (**H**) Kv1.3 mRNA relative expression in BMDCs. BMDCs from WT (Cd11c-Cre-GFP) and KO (*Dlg1*$^{fl/fl}$Cd11c-Cre-GFP) mice were purified by $CD11c^+$ cells and stimulated with LPS (100 ng/ml) for the indicated time periods. Data were pooled from three independent experiments (one mouse in each group and assayed in triplicated wells). (**I**) Representative voltage-gated currents recorded from WT BMDCs incubated with PAP-1 (5 μM). (**J**) Ca^{2+} influx in WT and Dlg1-KO BMDCs stimulated by LPS (200 ng/ml). Data are representative of two independent experiments assayed in triplicate.

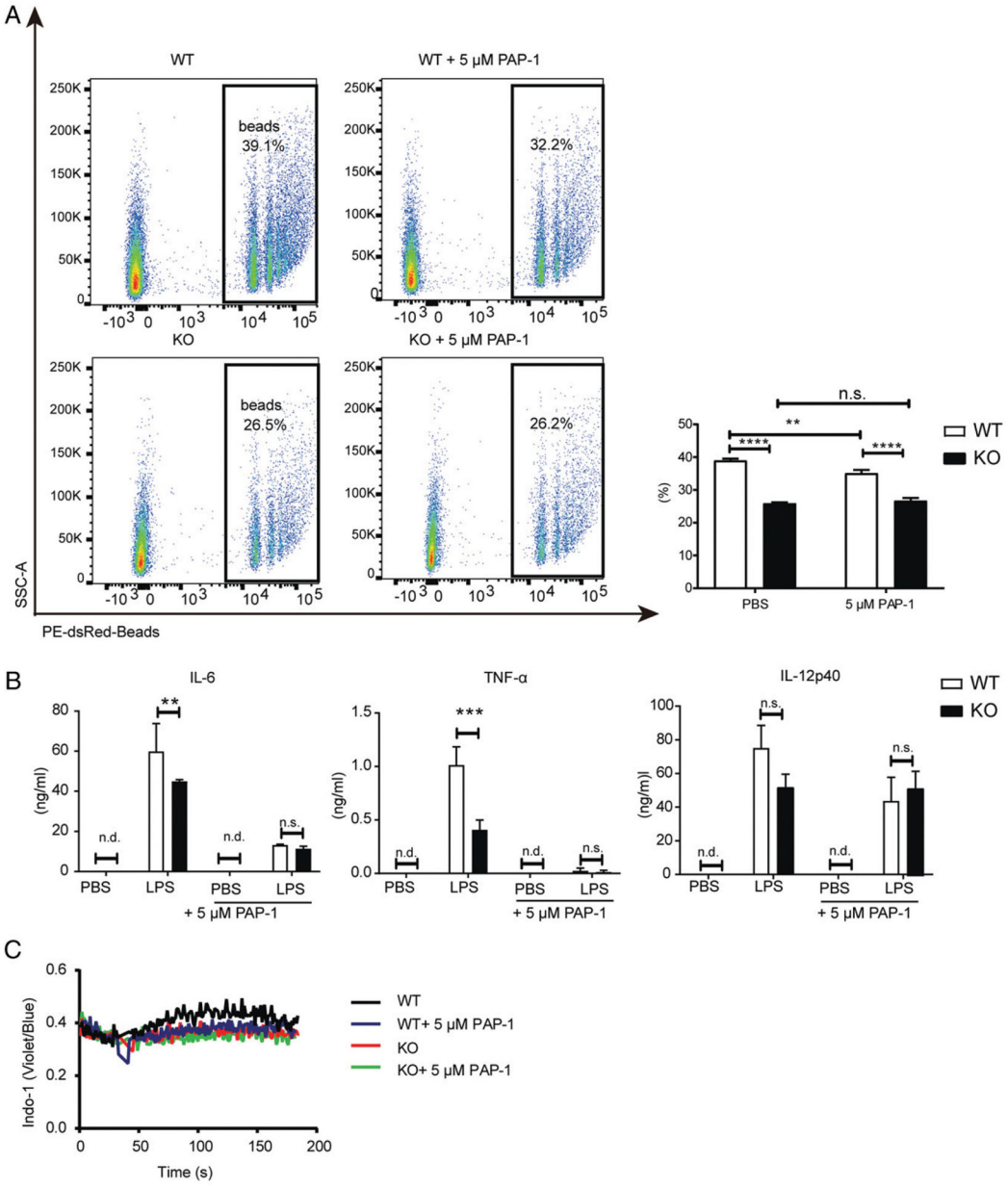

FIGURE 7.

Dlg1 is important for DC function in a Kv1.3-dependent manner. (**A**) Representative flow cytometric graphs (left panel) and quantification (right panel) of phagocytosis of WT and Dlg1-KO BMDCs with or without PAP-1 (5 μM). BMDCs were incubated with IgG-coated latex beads for 3 h in the absence or presence of PAP-1 (5 μM). The percentages displayed were phagocytosed cells from $CD11c^+$ BMDCs. Data are representative of two independent experiments (one mouse in each group, assayed in quadruplicate wells). (**B**) IL-6, TNF-α, and IL-12p40 production by WT and Dlg1-KO $CD11c^+$ BMDCs upon stimulation with LPS (100 ng/ml) in the presence or absence of PAP-1 (5 μM) overnight. Supernatant was collected and subject to ELISA. Data were pooled from three mice assayed in triplicated wells. (**C**) Ca^{2+} influx in WT and Dlg1-KO $CD11c^+$ BMDCs stimulated by LPS (200 ng/

ml). In the PAP-1 group, BMDCs were preincubated with PAP-1 (5 μM) for 30 min and then washed with HBSS and incubated with Indo-1 in HBSS as in the other group. Data are representative of three mice assayed in triplicated wells, and two-way ANOVA was performed. $^{**}p < 0.01$, $^{***}p < 0.001$, $^{****}p < 0.0001$. n.d., not detected; n.s., not significant.